Flux Growth and Electronic Properties of $Ba_2In_5Pn_5$ (Pn = P, As): Zintl Phases Exhibiting Metallic Behavior

Josiah Mathieu,[†] Randall Achey,[†] Ju-Hyun Park,[‡] Kenneth M. Purcell,[‡] Stanley W. Tozer,[‡] and Susan E. Latturner*,[†]

Department of Chemistry and Biochemistry, Florida State University, Tallahassee, Florida 32306, and National High Magnetic Field Laboratory, 1800 East Paul Dirac Drive, Tallahassee, Florida 32310

Received June 6, 2008. Revised Manuscript Received June 28, 2008

$Ba_2In_5P_5$ and $Ba_2In_5As_5$ were grown from the reaction of barium and the pnictogen elements in indium flux. These Zintl phases feature a new structure type in orthorhombic space group *Pnma* (for the phosphorus analogue, $a = 17.2572(2)$ Å, $b = 4.1599(1)$ Å, $c = 17.4895(2)$ Å, $R_1 = 0.0376$). The layered structure features anionic slabs of interconnected main group atoms, with hexagonal channels defined by In−In bonds and capped on the outer edges by the pnictides; Ba^{2+} cations reside in between these layers. Despite the apparently charge-balanced nature of the structure and the band gaps indicated in density of states calculations, the rising resistivities with increasing temperature indicate these materials behave as metals (ρ_{RT} for $Ba_2In_5P_5 = 1.0 \times 10^{-3}$ Ω cm, and ρ_{RT} $Ba_2In_5As_5 = 6.1 \times 10^{-3}$ Ω cm). NMR studies of the ^{115}In Knight shifts and the Korringa relationship observed for the temperature dependence of the ^{31}P resonance of $Ba_2In_5P_5$ characterize these compounds as semiconductors doped into the metallic regime. The flux growth method is the likely source of doping.

Introduction

Traditional solid-state synthesis methods present several limitations when it comes to exploratory research: high temperatures must be used, and the most thermodynamically stable compound is generally formed. This method also typically leads to powders; in most cases, crystals can be formed only after lengthy annealing of the product. Use of molten metal fluxes is an appealing option for exploratory synthesis, as this is a lower-temperature technique that allows for isolation of kinetically stabilized or metastable phases.[1] Dissolution of the reactant elements in the flux enables reaction at low temperatures; after the reaction is complete, the flux can be removed by centrifugation or dissolved in acid. Indium has a low melting point of 157 °C as well as a large difference between its melting point and boiling point, which makes it a viable flux for reaction chemistry, and it can easily be separated from its products through centrifugation. Indium flux reactions have yielded metallic phases ($YbCoIn_5$, RCu_2Si_2, RIn_3) as well as semiconductor crystals (Ge, Si, InP).[1,2] In this work, they yield materials that seem to bridge these classifications—Zintl phases that appear to be poor metals.

Zintl phases are saltlike compounds in which electropositive metals donate their valence electrons to clusters or networks made up of electronegative metalloid elements that generally come from groups 13−15, but can occasionally include transition metals. They have a well-defined relationship between their chemical and electronic structures as explained by the Zintl−Klemm concept. Because of the fact that that the electropositive element is assumed to transfer all of its valence electrons to the electronegative elements, Zintl phases are considered to be closed-shell compounds.[3] They are therefore expected to be diamagnetic semiconductors (with the exception of those containing paramagnetic cations). A number of exceptions exist; for instance, $SrSn_3Sb_4$, $Ba_3Sn_4As_6$, and $EuIn_2P_2$ can be explained in terms of their bonding by the Zintl−Klemm concept, but they have been found to have a weakly metallic resistivity.[4−6] Metallic behavior is also observed in Zintl phases with small band gaps that are doped by impurities or slight variations in stoichiometry, such as the clathrate phases $Ba_8Ga_{16}Ge_{30}$ and $Ba_8Al_{15}Si_{31}$.[7,8]

In this work, we present $Ba_2In_5As_5$ and $Ba_2In_5P_5$, two Zintl phases with a new structure type. This structure can be rationalized by the Zintl−Klemm concept, and band structure calculations imply that the materials should be semiconductors. However, transport measurements indicate metallic behavior. NMR studies of Knight shifts and the Korringa relation—seldom investigated for Zintl phases—also support the classification of these compounds as poor metals. These

* Corresponding author. E-mail: latturne@chem.fsu.edu.
[†] Florida State University.
[‡] National High Magnetic Field Laboratory.

(1) Fisk, Z.; Remeika, J. P. *Handbook on the Physics and Chemistry of Rare Earths*; Gshneider , K. A., Eyring, L., Eds.; Elsevier Science: Amsterdam, 1989; Vol. 12.
(2) Kanatzidis, M. G.; Pottgen, R.; Jeitschko, W. *Angew. Chem., Int. Ed.* **2005**, *44*, 6996–7023.
(3) Kauzlarich, S. *Structure and Bonding of Zintl Phases and Ions*; VCH Publishers: New York, 1996.
(4) Lam, R.; Zhang, J.; Mar, A. *J. Solid State Chem.* **2000**, *150*, 371–376.
(5) Lam, R.; Mar, A. *Solid State Sci.* **2001**, *3*, 503–512.
(6) Jiang, J.; Kauzlarich, S. M. *Chem. Mater.* **2006**, *18*, 435–441.
(7) (a) Bryan, J. D.; Blake, N. P.; Metiu, H.; Stucky, G. D.; Iversen, B. B.; Poulsen, R. D.; Bentien, A. *J. Appl. Phys.* **2002**, *92*, 7281–7290. (b) Latturner, S. E.; Bryan, J. D.; Blake, N.; Metiu, H.; Stucky, G. D. *Inorg. Chem.* **2002**, *41*, 3956–3961.
(8) Condron, C. L.; Martin, J.; Nolas, G. S.; Piccoli, P. M. B.; Schultz, A. J.; Kauzlarich, S. M. *Inorg. Chem.* **2006**, *45*, 9381–9386.

10.1021/cm8015353 CCC: $40.75
Published on Web 08/16/2008

data are evaluated in light of previous reports on metallic Zintl phases and the potential for doping inherent in the flux growth technique.

Experimental Section

Synthesis. $Ba_2In_5As_5$ was originally made in a reaction of the elements Ba, In, Ge, and As in a 0.5:15:1:1 mmol ratio with indium acting as a flux. Starting materials for the preparation of this compound were Ba rods (Acros-Organics, 99+%), In shot (Alfa-Aesar, 99.9%), Ge powder (Cerac, 99.999%), and As powder −20 mesh (Cerac, 99%). Because of the toxicity of arsenic, gloves and masks were used when handling the reactant and the reactions were carried out in a furnace located in a hood. All elements were combined in an alumina crucible with half the indium flux loaded on the bottom and half on top of the rest of the reactants. The crucible was placed in a fused silica tube; another alumina crucible was filled with Fiberfrax ceramic fiber and inverted on top of the reaction crucible in the silica tube to act as a filter during centrifugation. The fused silica tube was sealed under a vacuum of 1×10^{-2} Torr, and then heated to 1000 °C in 10 h, held at this temperature for 48 h, cooled to 850 °C in 150 h, held for 24 h, cooled to 800 °C in 50 h, held for 24 h, cooled to 700 °C in 50 h, held for 24 h, and finally cooled to 600 °C. At this temperature, the silica tubes were removed from the furnace, inverted and quickly placed in a centrifuge to remove excess molten flux from the mass of needle shaped crystalline product. Many of the crystals are covered with patches of indium flux. Small amounts of InAs and barium arsenide phases are also obtained as side products.

Elemental analysis was performed on the crystals using a JEOL 5900 scanning electron microscope (SEM) with energy-dispersive spectroscopy (EDS) capabilities. The crystals were mounted on carbon tape and analyzed using a 30 kV accelerating voltage and an accumulation time of 10−20 s. An average of eight crystals gave a rough stoichiometry of $Ba_1In_3As_4$. Because germanium was not incorporated into the product, the synthesis was done again without this element, heating at 60 °C/h to 1000 °C, holding for 48 h, cooling at 2 °C/h to 600 °C, and then centrifuging.

$Ba_2In_5P_5$ was synthesized the same way using phosphorus (Alfa-Aesar, 99%) instead of arsenic, and with a modification of the previous heating profile. The reaction tube was heated at 60 °C/h to 500 °C, and held there for 1 h to facilitate mixing; heating continued at 60 °C/h to 1100 °C, where the reaction was kept for 48 h. It was then cooled at 2 °C/h to 600 °C and centrifuged. EDS analysis yielded a rough stoichiometry of $Ba_2In_7P_7$ for an average of 5 crystals. Crystals of InP are typically obtained as side-products from this reaction, as well as some as yet unidentified grayish-red powder. Attempts to make these phases from stoichiometric reactions of the elements failed, yielding instead InP and InAs.

Structure Refinements. Samples for X-ray diffraction were selected from the SEM plate after elemental analysis and fragments of the large needle shaped crystals were mounted on glass fibers for diffraction. Single-crystal X-ray diffraction data were collected at room temperature using a Bruker AXS SMART CCD diffractometer equipped with a Mo radiation source. Processing of the data was accomplished with the use of the program SAINT; an absorption correction was applied to the data using the SADABS program.[9] Refinement of the structure was performed using the SHELXTL package.[10] The crystallographic data is summarized in Tables 1 and 2. Additional details regarding the crystallographic refinements can be found in the Supporting Information. Powder X-ray diffraction data was collected on several samples using a Rigaku Ultima III Powder X-ray diffractometer with a Cu radiation source and a CCD detector.

Table 1. Crystallographic Data for $Ba_2In_5Pn_5$ Phases

	$Ba_2In_5P_5$	$Ba_2In_5As_5$
fw (g/mol)	1003.63	1223.38
space group	*Pnma*	*Pnma*
a (Å)	17.257(3)	17.461(2)
b (Å)	4.1599(6)	4.2905(4)
c (Å)	17.490(3)	17.961(2)
V (Å^3)	1255.5(3)	1345.6(2)
d_{calcd} (g/cm^3)	5.31	6.04
Z	4	4
T (K)	298	298
radiation	Mo Kα	Mo Kα
$2\theta_{max}$	56.56	56.62
index ranges	$-22 \le h \le 22$ $-5 \le k \le 5$ $-22 \le l \le 23$	$-23 \le h \le 23$ $-5 \le k \le 5$ $-23 \le l \le 23$
no. of reflns collected	16 653	17 871
unique data/params	1770/73	1894/74
μ (mm^{-1})	15.8	26.3
R_1/wR_2[a] ($I > 4\sigma(F_o)$)	0.0376/0.0690	0.0390/0.0844
R_1/wR_2 (all data)	0.0464/0.0718	0.0404/0.0850
residual peaks/hole	2.13/−1.49	5.39/−1.91

[a] $R_1 = \sum(|F_o| - |F_c|)/\sum|F_o|$; $wR_2 = [\sum[w(F_o^2 - F_c^2)^2]/\sum(w|F_o|^2)^2]^{1/2}$.

Table 2. Atomic Positions for the $Ba_2In_5Pn_5$ Phases[a]

atoms	x	y	z	U_{eq}[b]
		$Ba_2In_5P_5$		
Ba1	0.01951(4)	1/4	0.62099(4)	0.0095(1)
Ba2	0.04209(4)	1/4	0.12983(4)	0.0134(2)
In1	0.15747(4)	1/4	0.81018(4)	0.0099(2)
In2	0.31328(4)	1/4	0.77710(4)	0.0095(2)
In3	0.17218(4)	1/4	0.44118(4)	0.0103(2)
In4	0.33002(4)	1/4	0.47180(4)	0.0103(2)
In5	0.28948(4)	1/4	0.12583(4)	0.0087(2)
P1	0.1044(2)	1/4	0.3087(2)	0.0086(5)
P2	0.3852(2)	1/4	0.0113(2)	0.0079(5)
P3	0.3919(2)	1/4	0.2354(2)	0.0088(5)
P4	0.5834(2)	1/4	0.5589(2)	0.0090(5)
P5	0.3023(2)	1/4	0.6253(2)	0.0083(5)
		$Ba_2In_5As_5$		
Ba1	0.02046(4)	1/4	0.62073(4)	0.0116(2)
Ba2	0.04258(4)	1/4	0.13045(4)	0.0150(2)
In1	0.15773(5)	1/4	0.81209(2)	0.0128(2)
In2	0.31191(5)	1/4	0.77898(5)	0.0125(2)
In3	0.17319(5)	1/4	0.44182(5)	0.0129(2)
In4	0.32928(5)	1/4	0.47149(5)	0.0132(2)
In5	0.28915(5)	1/4	0.12686(4)	0.0094(2)
As1	0.10370(7)	1/4	0.30931(7)	0.0104(3)
As2	0.38575(7)	1/4	0.01156(7)	0.0092(3)
As3	0.39297(7)	1/4	0.23718(7)	0.0103(3)
As4	0.58216(7)	1/4	0.55705(7)	0.0101(3)
As5	0.30407(7)	1/4	0.62603(6)	0.0088(3)

[a] All atoms are on 4c Wyckoff sites. [b] U_{eq} is defined as 1/3 of the trace of the orthogonalized U_{ij} tensor.

Differential Scanning Calorimetry−Thermogravimetric Analysis (DSC−TGA). DSC−TGA for $Ba_2In_5P_5$ and $Ba_2In_5As_5$ were performed using a TA instruments SDT 2960 Simultaneous DSC−TGA. A total of 30–40 mg sample masses of single crystals were placed in alumina sample containers; an empty alumina sample container was placed on the reference side of the detector. Each sample was heated under a N_2 gas stream to 1100 °C at 10 °C/min and held there for 5 min, followed by cooling at −10 °C/min to room temperature. After the analysis, the solid in the sample container was removed, ground to powder, and analyzed using powder X-ray diffraction.

Resistivity Measurements. DC conductivity measurements were performed on a Quantum Design PPMS. The surfaces of the crystals

(9) *SAINT*, version 6.02a; Bruker AXS: Madison, WI, 2000.
(10) Sheldrick, G. M. *SHELXTL NT/2000*, version 6.1; Bruker AXS: Madison, WI, 2000.

were carefully scraped to remove excess indium (attempting to remove the indium with an acid etch led to dissolution of the crystals). Contacts were made with gold wire and silver paste in a standard four-probe configuration along the *b*-axis of the crystals. The dimensions of the $Ba_2In_5As_5$ and $Ba_2In_5P_5$ crystals were $1 \times 0.013 \times 0.018$ and $1 \times 0.020 \times 0.024$ mm^3, respectively. A current of 200 and 2500 μA was used for $Ba_2In_5As_5$ and $Ba_2In_5P_5$, respectively. The measurements were run from 1.9 to 317 K. Minor kinks in the data around 250−260 K were seen in several samples and appear to be an artifact of annealing of the silver paste. No structural transitions for the title compounds were apparent in diffraction data taken in this temperature range.

Nuclear Magnetic Resonance. Magic angle spinning (MAS) NMR data were collected on a Varian Inova 500 widebore spectrometer. In an argon-filled drybox, crystals of $Ba_2In_5Pn_5$ phases were ground with KBr in 50:50 mixtures by volume to facilitate spinning; these mixtures were packed into 4 mm zirconia rotors sealed with airtight screwcaps. In between measurements the filled rotors were stored in the drybox. The external references used were 0.1 M aqueous $In(NO_3)_3$ for ^{115}In ($I = 9/2$, 95.84% abundant) and 15 M phosphoric acid for ^{31}P ($I = 1/2$, 100% abundant). Data was collected at room temperature and a spinning rate of 5kHz, using a one-pulse sequence (pulse length 5 μs and relaxation delay 500 ms).

The temperature dependence of the ^{31}P T_1 relaxation time of $Ba_2In_5P_5$ was investigated to further explore the possibly metallic nature of the material by determining if the Korringa relation was followed. T_1 values were measured using the inversion recovery method. Data was collected over a temperature range from 144.9 to 323.2 K with a spinning rate of 5 kHz. During variable temperature operation of the spectrometer, the temperature controlling gas as well as the MAS probe is run completely with nitrogen (as opposed to air under normal conditions) in order to achieve low temperatures as well as prevent oxidation of sensitive electronics at high temperatures. To maintain proper temperature equilibration, we performed constant flow rate monitoring.

Electronic Structure Calculations. Density functional theory-based electronic structure calculations were performed on both compounds using the linear muffin tin orbital method within the local spin density approximation.[11] Atom positions from the experimental crystal structures were used as inputs for the calculations, which were performed on a $4 \times 12 \times 4$ *k*-point grid (63 irreducible *k*-points).

Results and Discussion

Flux synthesis in an excess of indium seems to be required to isolate the title phases. Stoichiometric reactions led to indium phosphide or indium arsenide as predominant products, with no evidence of the $Ba_2In_5Pn_5$ phases in the powder XRD patterns. The failure of stoichiometric synthesis is evidence that these phases are metastable or peritectic in nature; this is also indicated by their melting point behavior (vide infra). Flux synthesis is known to facilitate the isolation of such materials.[1,2] InP and InAs are also produced in the flux syntheses, comprising up to 30−40% of the solid product; the triangular crystals are easily distinguishable from the needle shaped Zintl phase crystals. In the arsenide synthesis, use of higher soak temperatures (1000 °C) seems to promote formation of more of the Zintl phase and less InAs (5–10% of the solid product).

(11) Jepsen, O.; Andersen, O. K. STUTTGART TB-LMTO-ASA Program, version 47; Max-Planck-Institut für Festkörperforschung: Stuttgart, Germany, 2000.

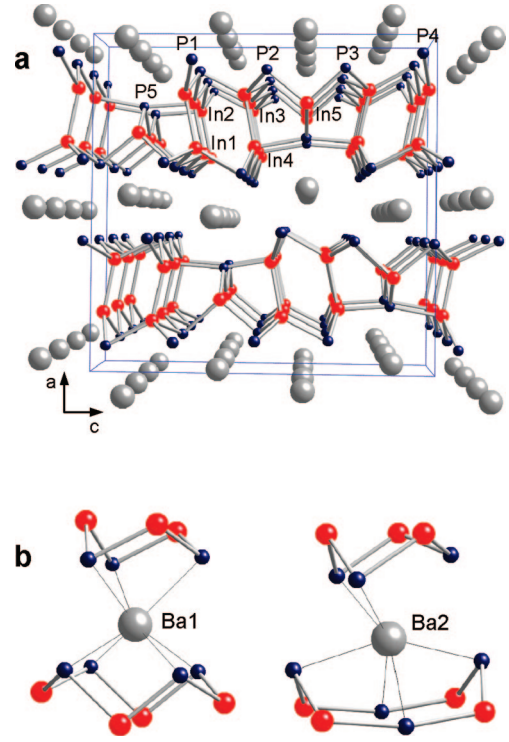

Figure 1. (a) $Ba_2In_5Pn_5$ structure, viewed down the *b*-axis. Large gray spheres are Ba; small dark blue spheres are pnictogen atoms; and red spheres are indium atoms. (b) Coordination environment of the two barium sites.

The $Ba_2In_5Pn_5$ compounds form as very thin silvery needles with metallic luster. In crystalline form they are somewhat stable to water and dilute acids due to formation of an oxide coating, indicated by a reddish coloration on the crystal surface. In powder form, the phosphide compound degrades in air rapidly; the arsenide is more robust. $Ba_2In_5P_5$ is stable under nitrogen until about 900 °C when the mass of the sample began to decrease slightly, possibly due to evaporation of excess indium flux coating the crystals. At 935 °C the melting point is reached. A recrystallization is seen at 902 °C; however, the XRD pattern of the product after this process indicates a mixture of predominantly InP and In metal. The compound is therefore incongruently melting. $Ba_2In_5As_5$ appears to melt at 889 °C, again accompanied by crystallization at 863 °C into InAs and other unidentifiable phases.

Syntheses of analogues with divalent metals Sr and Eu were explored, as was replacement of phosphorus and arsenic with the heavier elements in the pnictide family. Attempts to make Sr and Eu analogues resulted in phases with the hexagonal $EuIn_2P_2$ structure type instead[6] ($P6_3/mmc$, $a = 4.2055(3)$ Å, $c = 17.887(2)$ Å for $EuIn_2As_2$; $a = 4.0896(3)$ Å, $c = 17.783(3)$ Å for $SrIn_2P_2$; and $a = 4.2145(7)$ Å, $c = 18.067(6)$ Å for $SrIn_2As_2$). InAs and InP were also observed products. An antimony analogue $Ba_2In_5Sb_5$ could not be obtained; instead, a highly air-sensitive barium antimonide phase formed.

Structure. The two title phases have a new structure type (shown in Figure 1) which can be analyzed using the standard Zintl−Klemm charge balancing rules. The two crystallographically distinct barium atoms donate their valence electrons to the main group element layer. The structure can thus be understood as comprising anionic slabs separated

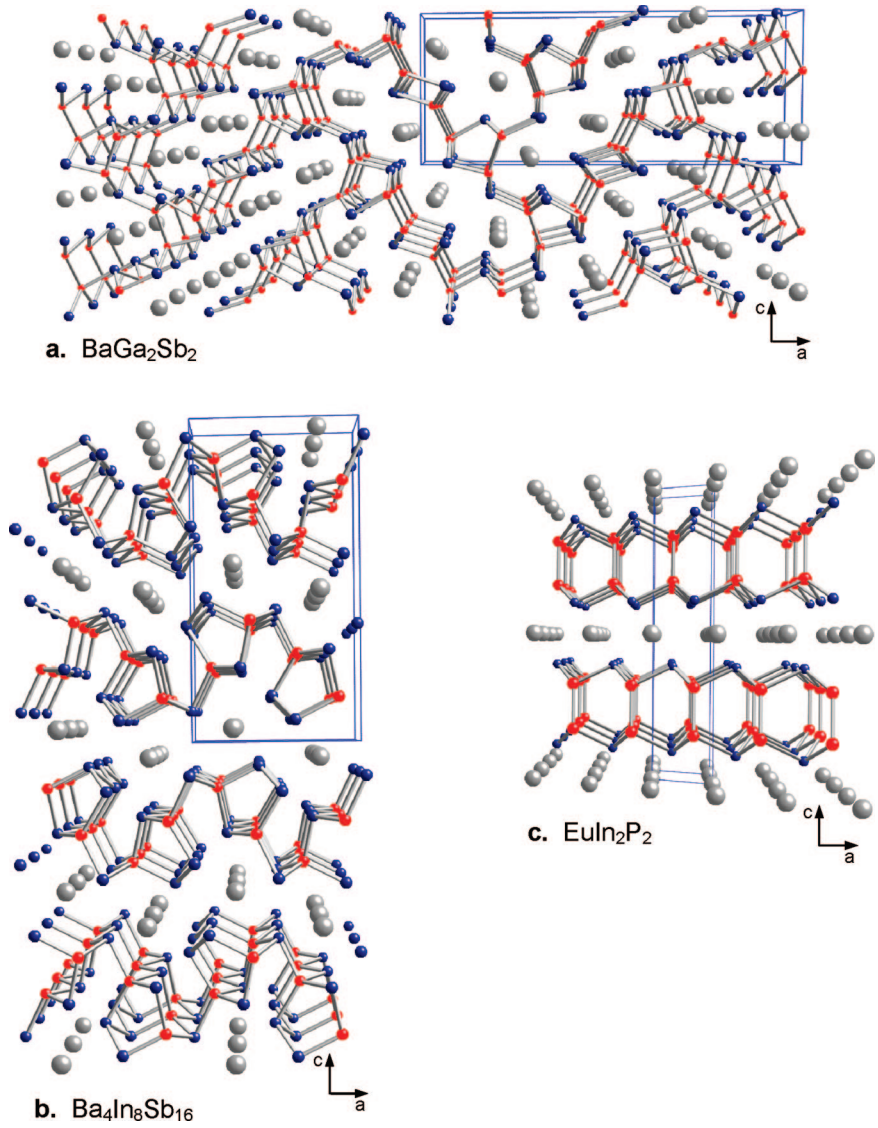

Figure 2. Other II−III−V Zintl phase structures. (a) $BaGa_2Sb_2$ features pentagonal channels defined by Ga−Ga bonds; the ethane-like building block Sb_3Ga-$GaSb_3$ is a common motif. (b) $Ba_4In_8Sb_{16}$ structure also features pentagonal channels but these contain Sb−Sb bonds. (c) $EuIn_2P_2$ structure features hexagonal channels defined by $P_3In-InP_3$ units.

by layers of Ba^{2+} cations. In the anionic main group slabs, all of the indium atoms (there are 5 unique In sites; see Table 2) have roughly tetrahedral coordination. Because they are bonded to 4 atoms, the In can be thought of as In^-. Among the five pnictide sites, four of them are in capping sites for the anionic layer, coordinated to 3 indium atoms, and are therefore neutral in the charge counting scheme. The remaining Pn site, Pn(5), is in a very distorted tetrahedral arrangement, bonded to 4 In atoms, and has a +1 charge by the Zintl−Klemm counting rules. The overall charge balancing scheme is therefore $(Ba^{2+})_2[(4b\text{-}In^-)_5(4b\text{-}Pn^+)(3b\text{-}Pn^0)_4]^{4-}$.

This structure resembles other Zintl phases comprising similar elements. Many compounds have been synthesized from the combination of a divalent cation (Eu, Ba, Sr), a group III or trielide metal (Ga, In), and a group V or pnictide metalloid (P, As, Sb; use of arsenic is less common presumably because of toxicity). The importance of different synthetic methods is demonstrated by the fact that new compounds continue to be discovered in this phase space. Materials with a high ratio of M^{2+}: main group (such as Sr_3InAs_3, $Ba_3In_2P_4$, and $Ba_{14}InP_{11}$) have structures with anionic 1D ribbons of main group elements, usually comprised of trielide centered tetrahedra (units such as InP_4) linked together, surrounded by M^{2+} cations.[12] Compounds with a lower M^{2+}: main group ratio, such as the title compounds, tend to feature 2D layers or 3D networks of linked main group elements. The structures of $EuIn_2P_2$, $BaGa_2Sb_2$, and $Ba_4In_8Sb_{16}$ are shown in Figure 2 for comparison.[6,13] In general, the trielide element is tetrahedrally coordinated, and the divalent metal cation is coordinated by the more electronegative pnictide element. The coordination environment for the two Ba sites in $Ba_2In_5P_5$ is shown in

(12) (a) Cordier, G.; Schäfer, H.; Stelter, M. *Z. Naturforsch.* **1986**, *41b*, 1416–1419. (b) Cordier, G.; Schäfer, H.; Stelter, M. *Z. Naturforsch.* **1987**, *42b*, 1268–1272. (c) Somer, M.; Carrillo-Cabrera, W.; Peters, K.; von Schnering, H. G. *Z. Kristallogr.* **1998**, *213*, 4. (d) Carrillo-Cabrera, W.; Somer, M.; Peters, K.; von Schnering, H. G. *Chem. Berichte* **1996**, *129*, 1015–1023.

(13) (a) Park, S. M.; Kim, S. J.; Kanatzidis, M. G. *J. Solid State Chem.* **2003**, *175*, 310–315. (b) Kim, S. J.; Kanatzidis, M. G. *Inorg. Chem.* **2001**, *40*, 3781–3785. (c) Kim, S. J.; Hu, S.; Uher, C.; Kanatzidis, M. G. *Chem. Mater.* **1999**, *11*, 3154–3159.

Table 3. Selected Bond Lengths (Å)

	$Ba_2In_5P_5$	$Ba_2In_5As_5$
Ba1−Pn	3.227(2), 3.266(2), 3.272(2), 3.275(3)	3.299(1), 3.336(1), 3.344(1), 3.356(1)
Ba2−Pn	3.249(2), 3.307(3), 3.377(3), 3.398(2), 3.503(3)	3.329(1), 3.385(2), 3.432(1), 3.438(2), 3.532(2)
In−In	2.750(1), 2.776(1)	2.757(1), 2.777(1)
In−Pn	2.579(2) to 2.617(2)	2.6590(9) to 2.695(2)
In−Pn5	2.614(2), 2.662(3), 2.727(3)	2.6929(9), 2.751(2), 2.811(2)

Figure 1. Ba(1) interacts with seven P atoms with bond lengths ranging from 3.226 to 3.275 Å. Ba(2) has a distorted octahedral coordination to six P atoms at longer distances in the 3.249−3.398 Å range, with a seventh phosphorus atom at a distance of 3.503 Å (see Table 3). The longer distances around Ba(2) reflect the vicinity of this cation to the distorted tetrahedral phosphorus site, which has its own formal positive charge according to the Zintl−Klemm counting rules.

Other structural features common to the title compounds and the other II/III/V Zintl phases are trielide–trielide bonds and resulting pentagonal and hexagonal channels in the structure. In $Ba_2In_5Pn_5$, ethane-like $Pn_3In-InPn_3$ linkages are aligned parallel to each other and bridged by pnictogen atoms; this produces hexagonal channels along the *b*-axis direction. The In−In bond lengths are almost identical in the phosphide and arsenide, ranging from 2.75 to 2.78 Å. The Pn_3M-MPn_3 unit is also observed in the $BaGa_2Sb_2$ and $EuIn_2P_2$ structure types, with the latter having a similar In−In bond length to the compounds studied here. $Pn_3In-InPn_3$ linkages also form sections of the pentagonal channels of $Ba_2In_5Pn_5$; these pentagons include the highly distorted tetrahedral Pn(5) site. The distortion is reflected in both the angles and the bond lengths; for instance, most of the In−P bonds in the phosphide compound are in the 2.58−2.62 Å range, but the bonds to the P(5) atom include two longer bonds of 2.662(3) and 2.727(3) Å.

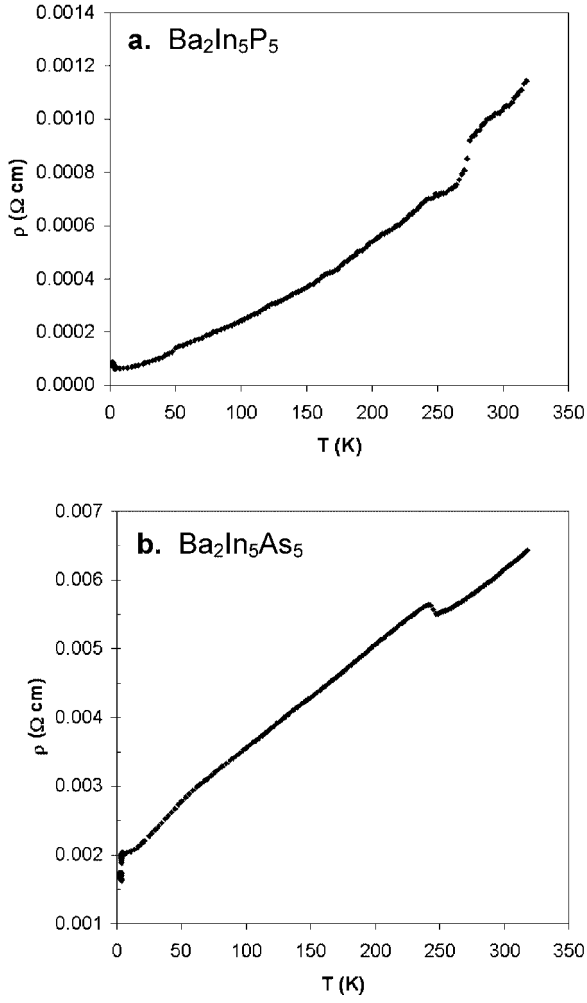

Figure 3. Single-crystal electrical resistivity data for the $Ba_2In_5Pn_5$ phases.

Transport Properties. The single-crystal resistivity data for both $Ba_2In_5P_5$ and $Ba_2In_5As_5$ show the temperature dependence characteristic of metallic materials (Figure 3). The phosphorus analogue has a room temperature resistivity almost an order of magnitude lower than the arsenic phase; $\rho_{RT} = 6.1 \times 10^{-3}$ Ω cm for $Ba_2In_5As_5$ and $\rho_{RT} = 1.0 \times 10^{-3}$ Ω cm for $Ba_2In_5P_5$. The poor metal nature observed for these materials is unusual for technically charge-balanced Zintl phases, which are normally semiconductors. It is also surprising that the phosphide is more conducting than the arsenide (this was reproducible over several samples); use of a heavier element in a semiconductor usually leads to a smaller band gap and lower resistivity. Indium flux occlusions within the $Ba_2In_5Pn_5$ crystals or on the surface are evidenced by the observation of traces of superconductivity at 3 K, but it is unlikely that these are acting as complete electrical shorts, given that the measured resistivity above 3 K is much higher than that of metallic indium.

NMR Studies. NMR measurements were carried out to further investigate the electronic properties of the $Ba_2In_5Pn_5$ materials and determine if the observed conductivity was a result of occlusions or characteristic of the bulk phase. The interaction of conduction electrons with an applied magnetic field produces an extra effective field on the nuclear magnetic moment, resulting in a large paramagnetic shift—the Knight shift.[14] Likewise, conduction electrons in a metal have a characteristic effect on the temperature dependence of the relaxation of the nuclear spins; this is observed as a linear dependence of the inverse of the spin−lattice relaxation time T_1 with temperature T and is known as the Korringa relation.[15]

The ^{115}In chemical shifts observed for the title compounds (referenced to aqueous $In(NO_3)_3$ at 0 ppm) are 625 ppm for $Ba_2In_5As_5$ and 799 ppm for $Ba_2In_5P_5$. The five indium sites in the crystal structure should lead to five peaks in the ^{115}In NMR spectrum, but only one broad peak is seen. This is likely due to the large quadrupole moment of indium nucleus and the similar but highly asymmetric sites of the indium atoms in the lattice. The magnitudes of the shifts are smaller

(14) (a) Carter, G. C.; Bennett, L. H.; Kahan, D. J. *Metallic Shifts in NMR—Review of Theory and Comprehensive Critical Data Compilation of Metallic Materials*; Progress in Materials Science; Pergamon-Elsevier Science: Oxford, U.K., 1977; Vol. 20.
(15) Slichter, C. P. *Principles of Magnetic Resonance*, 3rd ed.; Springer-Verlag: Weinheim, Germany, 1991.

than those seen for pure indium metal in bulk or occlusion form (ca. 8000 ppm) and are also well below the values reported for indium intermetallics such as $AuIn_2$, NiIn, and Li_3In, which tend to range from 3000−9000 ppm.[14,16−19] However, the observed shifts are much larger than the negative values or small positive values seen for ionic indium (as observed for InX_4^- ions in solution, where X = halide).[20] Shifts in the 300−800 ppm range have been observed for indium in III−V semiconductors; however, these shifts are very dependent on doping.[21,22] The 600−800 ppm range observed for the $Ba_2In_5Pn_5$ compounds can be roughly assigned to the doped semiconductor/poor metal regime, with the higher shift of the phosphide reflecting its higher conductivity compared to the arsenide.

For further characterization, ^{31}P data for $Ba_2In_5P_5$ at various temperatures were collected to investigate the Korringa effect. The room temperature ^{31}P resonance is observed at −180 ppm relative to phosphoric acid reference at 0 ppm; this shift remains constant at temperatures ranging from 144.9 to 323.2 K. Again, only one broad peak is observed, although it shows significant asymmetry (see Figure S2, Supporting Information). This may indicate slightly different chemical shifts for the five phosphorus sites, as would be expected comparing the distorted tetrahedral environment of P(5) to the more regular trigonal environments of the other four phosphorus atoms. The value of the chemical shift is close to the range observed for phosphorus in small band gap semiconductors such as $CdSnP_2$, $ZnSiP_2$, and $Sn_{17}Zn_7P_{22}I_8$ (−30 to −170 ppm).[23,24] The unusually short T_1 relaxation time observed for the ^{31}P nuclei in this material (ca. 1×10^2 ms) is several orders of magnitude faster than normally seen for this nucleus; this is an indication of rapid relaxation caused by conduction electrons. The temperature dependence of this relaxation time is also characteristic of a metal, as it follows the linear Korringa relationship (see Figure 4). These data also support the classification of $Ba_2In_5P_5$ as a poor metal or heavily doped semiconductor.

Electronic Structure Calculations. Band structure calculations were carried out on the $Ba_2In_5Pn_5$ phases to determine if the apparent metallic behavior is due to structural features or impurities. As shown in Figure 5, based on the crystal structure, these compounds are expected to be semiconductors, with a band gap of 0.6 eV for the phosphide and 0.4 eV for the arsenide. This indicates that impurities

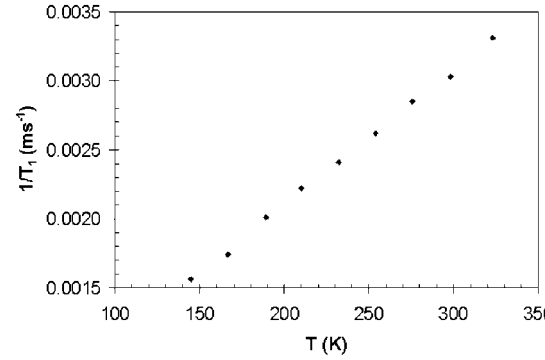

Figure 4. Plot of inverse ^{31}P spin−lattice relaxation vs temperature. The linearity of the data agrees with the Korringa relation and indicates that $Ba_2In_5P_5$ has metallic conductivity.

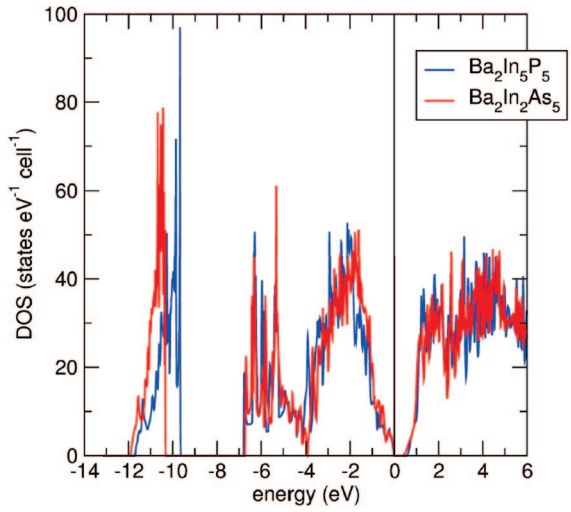

Figure 5. Total density of state calculations for $Ba_2In_5Pn_5$ phases. The Fermi level is set at 0 eV.

or structural defects act as dopants and result in the metallic conductivity evidenced in the transport measurements and NMR data.

Although most Zintl phases reported in the literature are by all measures semiconductors, there have been several cases where metallic resistivity was observed. These compounds are either very small band gap semiconductors, doped semiconductors, or true metals. $EuIn_2P_2$ has a resistivity of $\rho_{RT} = 2 \times 10^{-3}$ Ω cm and the temperature dependence typical of a metal at high temperatures. However, data at low temperatures makes it apparent that this can be attributed to thermal excitation across a very small band gap.[6] Doped semiconducting behavior—leading to metallic resistivity data—has been observed in some off-stoichiometry or deliberately doped Zintl phases. One example is $Eu_5In_{2-x}Zn_xSb_6$, a zinc-doped variant of the semiconducting $Eu_5In_2Sb_6$ parent phase.[25] Off-stoichiometry is a common occurrence in clathrate Zintl phases; the presence of framework vacancies and small changes from the ideal charge-balanced stoichiometry $Ba_8M_{16}T_{30}$ (M = trielide such as Al, Ga; T = tetrelide such as Si, Ge) leads to metallic behavior in $Ba_8Al_{14}Si_{31}$ and $Ba_8Ga_{16-x}Ge_{30+x}$. These phases can also be deliberately doped to produce metallic variants, as in the

(16) Charnaya, E. V.; Tien, C.; Kumzerov, Y. A.; Fokin, A. V. *Phys. Rev. B* **2004**, *70*, 052201.
(17) Van der Marel, C.; Brandenburg, E. P.; van der Lugt, W. *J. Phys. F: Met. Phys.* **1978**, *8*, L273–276.
(18) Wagner, T.; Gotz, S.; Masuhara, N.; Eska, G. *Phys. B: Condens. Matter* **1994**, *194−196*, 333–334.
(19) Bastow, T. J.; West, G. W. *J. Phys.: Condens. Matter* **2003**, *15*, 8389–8406.
(20) Harris, R. K. and Mann, B. E. *NMR and the Periodic Table*; Academic Press: London, 1979.
(21) Han, O. H.; Kuyng, H.; Timken, C.; Oldfield, E. *J. Chem. Phys.* **1988**, *89*, 6046–6052.
(22) Jung, W. S.; Han, O. H.; Chae, S. A. *Mater. Lett.* **2007**, *61*, 3413–3415.
(23) Lock, H.; Xiong, J.; Wen, Y. C.; Parkinson, B. A.; Maciel, G. E. *Solid State Nucl. Magn. Reson.* **2001**, *20*, 118–129.
(24) Kovnir, K. A.; Shatruk, M. M.; Reshetova, L. N.; Presniakov, I. A.; Dikarev, E. V.; Baitinger, M.; Haarmann, F.; Schnelle, W.; Baenitz, M.; Grin, Y.; Shevelkov, A. V. *Solid State Sci.* **2005**, *7*, 957–968.
(25) Park, S. M.; Choi, E. S.; Kang, W.; Kim, S. J. *J. Mater. Chem.* **2002**, *12*, 1839–1843.

$Ba_8Ga_{16+x}Sb_xGe_{30-2x}$ series of compounds.[7,8] On the other hand, the Zintl phases $SrSn_3Sb_4$ and $Ba_3Sn_4As_6$ are reported as being true metals. Their resistivity is similar to that of the title compounds (in the 1×10^{-3} Ω cm range), also increasing with temperature. But the lack of a band gap in these tin-containing phases is confirmed by DOS calculations and is attributed to band broadening due to the heavy main group elements and structural features that cross-link the channel structures.[4,5]

The exact nature of the defects that cause metallic behavior in the title $Ba_2In_5Pn_5$ phases is currently unknown, but it is likely that they are slightly off-stoichiometry, or doped with very small amounts of impurities. Since these compounds were grown from indium flux, the presence of excess indium in the structure, substituting on pnictide sites, is a possibility. The semiquantitative SEM-EDS elemental analysis technique is not accurate enough to determine small stoichiometry variations. The level of substitution is also too low to be seen in the crystal structure refinement. During the final cycles of the structure solution, the occupancies of all the atoms were allowed to vary and did not change significantly from unity. Low levels of doping/substitution would be averaged out in a crystal structure, but might be enough to result in metallic behavior.

Flux synthesis as a source of stoichiometry variations has not been greatly investigated. In the case of Zintl phases, such defects are particularly surprising because the products are expected to be charge balanced. However, in several of the aforementioned cases, a certain level of flexibility is available in the anionic framework, allowing for incorporation of different elements (Zn in the $Eu_5In_2Sb_6$ case, Sb in the $Ba_8Ga_{16}Ge_{30}$ case) as well as vacancies and substitutions.[7,8,25] It is notable that the off-stoichiometry clathrate phase $Ba_8Al_{14}Si_{31}$ is synthesized in aluminum flux, and the doped $Ba_8Ga_{16+x}Sb_xGe_{30-2x}$ series are grown in gallium flux. It is clearly possible that in this work, synthesis in indium flux may have led to $Ba_2In_{5+x}Pn_{5-x}$, a slightly off-stoichiometry metallic variant of the ideal semiconducting phase. Work is currently being carried out to synthesize the undoped $Ba_2In_5Pn_5$ compounds.

Acknowledgment. This research was supported by the FSU Department of Chemistry and Biochemistry and by the National Science Foundation (Grant DMR-05-47791). Transport measurements were carried out using the Open Door Laboratory facilities of Stanley Tozer's research group in the National High Magnetic Field Laboratory (with support from NSF Cooperative agreement DMR-0084173). We appreciate the assistance of Ram Seshadri (UCSB Materials Research Laboratory) in providing electronic structure calculations. We thank Sophia Hayes (Washington University) for useful discussions.

Supporting Information Available: Representative NMR spectra (^{31}P and ^{115}In MAS data) (PDF). Crystallographic collection parameters and tables of atomic positions, thermal parameters, bond lengths, and angles for the title compounds are available in CIF format. This material is available free of charge via the Internet at http://pubs.acs.org.

CM8015353